Successive Spray Deposition of P3HT/PCBM Organic Photoactive Layers: Material Composition and Device Characteristics

Alaa Abdellah, Kulpreet Singh Virdi, Robert Meier, Markus Döblinger, Peter Müller-Buschbaum, Christina Scheu, Paolo Lugli, and Giuseppe Scarpa*

Controlling the active layer composition in organic electronic devices represents one of the major challenges in their fabrication. In particular, the composition of mixed donor/acceptor active layers for photosensitive device applications is known to strongly influence device performance. Here, an alternative approach for the preparation of organic heterojunction photoactive layers by successive spray deposition of the donor material, poly(3-hexylthiophene) (P3HT), and acceptor material, [6,6]-phenyl C61-butyric acid methyl ester (PCBM), is reported. Optical absorption spectra, X-ray reflectivity, and cross-sectional transmission electron microscopy investigations are used to indicate the penetration of PCBM into a previously deposited P3HT layer and the spontaneous formation of a bulk heterojunction (BHJ) within the active layer, which provides the large interfacial area needed for efficient exciton dissociation. It is shown that organic photodiodes composed of photoactive layers prepared using this fabrication method exhibit a performance comparable to conventional BHJ devices in which the active layer is rigorously blended in advance. Moreover, separate handling of the individual materials and their deposition from distinct solutions enables an enhanced control of the active layer composition and hence increases the ability of tuning device characteristics.

1. Introduction

Organic solar cells and photodiodes have been subject of extensive research in recent years. Independent of the application of the photosensitive device, designs based on the bulk heterojunction (BHJ) concept showed the best performance. There a photoactive conjugated polymer is intimately blended with an electron acceptor, usually a fullerene, to form an interpenetrating network of both materials. The large interfacial area leads to efficient exciton dissociation at the interfaces and increases external quantum efficiency. Different studies have shown that device performance strongly depends on the morphology of the blend film, which is in turn related to the processing conditions.[1–3] Major drawbacks of the BHJ approach however are related to issues of carrier extraction rather than exciton diffusion and dissociation. Paths of a single material, donor or acceptor, forming continuous connections between anode and cathode lead to a decreased shunt resistance. Isolated islands of any of the two materials lead to trapping of carriers, which then do not contribute to the photocurrent. Vertical composition gradients resulting from the segregation of the donor material towards the anode interface and the acceptor material towards the cathode interface are believed to be beneficial for device performance. This is considered to be a result of efficient exciton dissociation due to intimate intermixing of the components as well as efficient charge transport and enhanced electrode selectivity.

Campoy-Quiles et al. used optical techniques to probe the final morphology of P3HT:PCBM films fabricated using different procedures.[4] They demonstrated that different treatments of P3HT:PCBM blends all lead to a common arrangement of the components, which consists of a vertically and laterally phase-separated blend of crystalline P3HT and PCBM. A simple method for improving the unfavorable vertical composition gradients of P3HT and PCBM in the photoactive layer of BHJ solar cells was proposed by Liang et al.[5] There a thin layer of P3HT was deposited on top of the PEDOT:PSS prior to spin-coating the P3HT:PCBM blend, resulting in enhanced electron blocking at the anode side, efficiency of photoinduced electron transfer and photocurrent of the device. PCBM was chosen by Kumar et al. as the acceptor material to be thermally deposited on top of the P3HT:PCBM active layer to achieve a vertical composition gradient in the BHJ structure.[6] The

A. Abdellah, Prof. P. Lugli, Dr. G. Scarpa
Institute for Nanoelectronics
Technische Universität München
Arcisstraße 21, 80333 Munich, Germany
E-mail: alaa.abdellah@tum.de
K. S. Virdi, Dr. M. Döblinger, Prof. C. Scheu
Department of Chemistry
Ludwig-Maximilians-Universität München
Butenandstrasse 11, 81377 Munich, Germany
R. Meier, Prof. P. Müller-Buschbaum
Lehrstuhl für Funktionelle Materialien
Physik-Department E13, Technische Universität München
James-Franck-Straße 1, 85747 Garching, Germany

DOI: 10.1002/adfm.201200548

observed increase in efficiency was attributed to improved transport and extraction of electrons near the cathode. Wang et al. fabricated a polymer photovoltaic device with P3HT/PCBM bilayers as active film with a concentration gradient by choosing the proper solvent system for each layer.[7] Since the solvent for the upper PCBM layer can partially swell the bottom P3HT layer, an intermixed zone with a concentration gradient of P3HT and PCBM is created between two layers. The devices showed an enhanced photocurrent density and power conversion efficiency compared to those of the bulk heterojunction PV prepared under the same fabrication condition. An almost identical experiment was conducted by Ayzner et al., leading to similar results but with a significantly different interpretation of those results.[8] They demonstrate that o-dichlorobenzene and dichloromethane serve nicely as a pair of orthogonal solvents from which sequential layers of P3HT and PCBM, respectively, can be spin-cast. Atomic force microscopy, various optical spectroscopies, and electron microscopy are reported to demonstrate that the act of spin-coating the PCBM overlayer does not affect the morphology of the P3HT underlayer, so that the authors claim to have a well-defined planar interface in their spin-cast P3HT/PCBM bilayers. This seems to be in strong contrast to the formation of the concentration graded bilayer shown by Wang et al. using an identical set of solvents.

Here we introduce an alternative approach for the preparation of organic heterojunction photoactive layers by successive spray deposition of the donor and acceptor materials comprising such a layer. Separate handling of the two materials and their deposition from distinct solutions provides a major degree of freedom in the formation of the active layer morphology/composition and hence in the ability of tuning device characteristics. Similar advantages were recently demonstrated by Chen et al. for organic solar cells fabricated by alternating spray deposition.[9] In contrast to their method, where the active layer is built by an alternating deposition of donor and acceptor materials to achieve intermixing of the components, we rely on a self-mixing of components inherent to our deposition routine, in addition to material interdiffusion occurring in the photoactive layer. Further, organic photodetectors with successively sprayed photoactive layers are fabricated. We demonstrate that rigorous blending of the two solutions prior to deposition is not necessary for obtaining good device performance. The blend required for the formation of a higher surface area at the heterojunction interface is shown to be created during deposition as a result of the deposition method employed here in combination with the thermal post-deposition treatment. Results presented are consistent with very recent data of morphology evolution in P3HT/PCBM bilayer model systems, where rapid interdiffusion of PCBM into P3HT upon thermal annealing is shown to result in the spontaneous formation of nanomorphologies equivalent to those in conventional BHJ systems.[10–12]

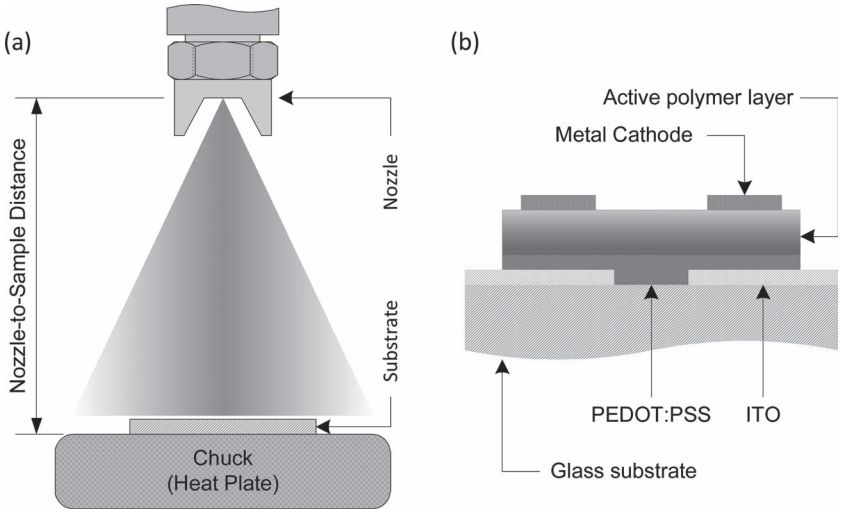

Figure 1. a) Schematic drawing of the experimental setup, indicating the vertical arrangement of nozzle and substrate. b) General device architecture of an organic photodiode illustrating the layer stack involved.

2. Results and Discussion

One of the major challenges in the fabrication of organic electronic devices based on solution-processable polymers is the successive deposition of multiple layers of different organic materials. The problem arises from the fact that many of these materials are soluble in the same set of solvents, making it rather complicated to implement even simple bilayer architectures directly deposited from solution. Depositing an additional layer on top of an existing one usually results in partial dissolving and/or swelling of the underlying layer due to the solvent present in the solution. The degree of dissolving strongly depends on solvent properties as well as deposition method involved in the process. Spray deposition is considered to minimize this issue due to the fast evaporation of the tiny droplets arriving at the substrate.[13–15] Here we demonstrate that successive spray deposition of the donor and acceptor materials of the photoactive layer in an organic photodiode, using the same solvent, still leads to significant intermixing of the materials allowing the formation of an interpenetrating network required for achieving performances comparable to those of conventional blend devices. **Figure 1**a shows a schematic drawing of the experimental setup used, indicating the vertical arrangement of nozzle and substrate. The general device architecture of our organic photodiode is illustrated in Figure 1b. One of the main advantages of spray deposition for this kind of process is the uniform distribution of small-volume droplets in the area of interest which in turn gives a uniform dissolving and intermixing over time and enables high reproducibility of the fabricated devices. This is in strong contrast to other deposition methods, such as spin-coating, where a large-volume solution is usually dispensed locally causing non-uniform dissolving of the underlying layer and hence poor reproducibility due to significantly longer interaction time with the solvent.

2.1. Partial Dissolving and Intermixing

As a first step towards the realization of a heterojunction with controlled morphology and/or composition by our proposed

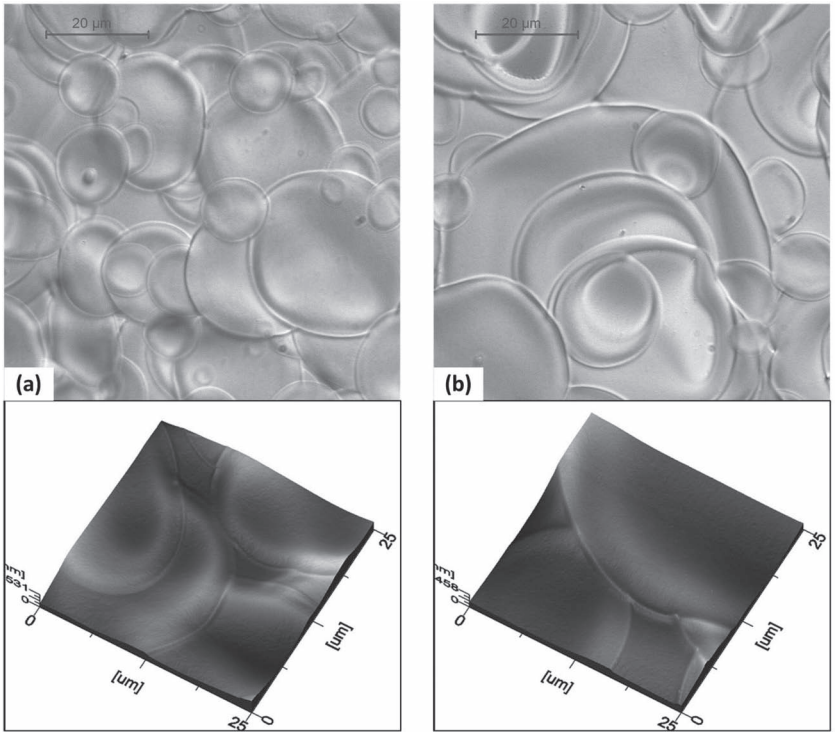

Figure 2. a) Optical and atomic force microscopy images of a spray deposited layer of pristine P3HT showing typical disk-like structures with heightened boundaries originating from dried solution droplets. b) Images of the same layer after spray deposition of pure dichlorobenzene, showing changed surface features and an increased average diameter of the droplet boundaries.

method of successive spray deposition, it is necessary to carefully examine the extent of partial dissolving and intermixing on previously deposited underlying layers and its implications on the integrity of this layer. For this purpose, P3HT was spray deposited from an o-dichlorobenzene (o-DCB) based solution directly onto a glass substrate to form a pristine layer of the donor material. In a following step, pure o-DCB was sprayed on top of the P3HT layer in a region well defined by shadow masking. Samples were then characterized by comparing optical as well as atomic force microscopy (AFM) images of unexposed and exposed regions of the P3HT layer. By spraying pure o-DCB it is possible to visualize the impact of solvent droplets hitting the surface of the polymer without having actual deposition of another material. **Figure 2**a shows the optical and AFM images of a protected area of the P3HT layer. One can clearly identify the typical disk-like structures with heightened boundaries formed upon impact of individual droplets on the substrate surface and their subsequent drying. The polymer layer is then built up by the stacking of such droplets which are assumed to merge to some extent by partial dissolving of previously deposited droplets.[15] For comparison, images of an unprotected area on the same sample are shown in Figure 2b. The most noticeable difference is a significantly increased average diameter of the droplet boundaries in the latter case. Changes in the general feature dimensions of the surface indicate a modification of the layer topography and/or morphology upon impact of the solvent droplets. This phenomenon is best described by the partial dissolving and subsequent resolidification of the polymer with redefined features, induced by wet solvent droplets hitting the polymer surface. Further, it can be seen that the penetration of droplets can reach the substrate at some points creating pinholes in the polymer layer. This indicates that locally the acceptor material will be directly in contact with the hole-extraction layer, in our case PEDOT:PSS. Nevertheless, globally the donor material concentration will remain predominant at this interface. Such a P3HT-rich layer at the hole-extraction interface should be beneficial for device performance as already described above. The extent of penetration and hence intermixing of the different layers strongly depends on spray parameters as well as solvent properties, providing means for tuning active layer morphology and device performance. However, an interaction with the residual solvent during deposition is expected to result in a coarse intermixing occurring at a scale close to that of the droplet dimensions.

Taking a close look at optical microscopy images of separately sprayed P3HT and PCBM layers reveals no significant difference in surface topography as both layers exhibit typical features of a spray deposited layer. This changes drastically after thermal post-deposition annealing, which does not show any visible modification of the P3HT layer while the PCBM layer shows strong crystallization over the entire area. The droplet boundaries present before annealing almost completely vanish in the thermally treated layer of PCBM. A similar behavior can be observed when spraying PCBM as acceptor material on top of a previously deposited layer of P3HT as donor material. Optical microscopy images of such a layer after thermal post-deposition treatment are shown in **Figure 3**. There are two main characteristics to be pointed out here, the density and size of the PCBM crystalline structures visible in the image. Compared to a conventional P3HT:PCBM blend layer spray deposited and thermally annealed under similar conditions,[15] this layer shows a significantly higher density of crystalline structures on the surface. Further, the structures are more pronounced with larger dimensions of up to 100 µm, thereby being around four to five times larger than their counterparts on a blend layer. This clear increase in density as well as size of PCBM crystalline structures on the surface of the sample indicates the existence of a high acceptor material concentration at the interface to the negative electrode. Such a PCBM-rich layer at the electron-extraction interface is expected to be beneficial for device performance.

2.2. Characteristics of Successively Sprayed Active Layers

Optical absorption spectra of pristine films (P3HT, PCBM) as well as composite films (pre-blended P3HT:PCBM, successively

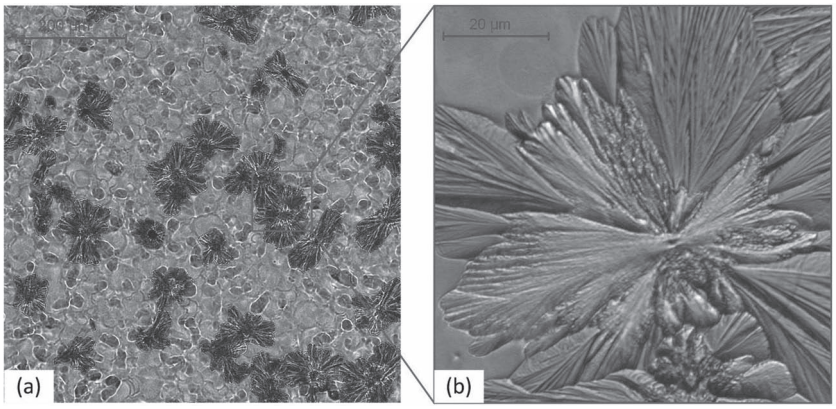

Figure 3. Optical microscopy image of a thermally annealed P3HT/PCBM layer prepared by successive spray deposition of the individual components (left). The details of a typical PCBM crystalline structure existing on the surface are shown in a zoom-in (right).

sprayed P3HT/PCBM) were examined and analyzed before and after thermal post-deposition treatment. **Figure 4**a shows the results obtained for pristine films while Figure 4b shows the results obtained for composite films. In case of the sprayed pristine P3HT and PCBM films, no clear changes in the spectrum can be observed after annealing, except for a slight increase in the absorption intensity. This is in close agreement with previously reported results for spin-coated layers.[16] Considering the blend film, one can clearly distinguish two main absorption peaks originating from PCBM around 345 nm and from P3HT around 500 nm. A main difference between as-prepared and annealed films lies in a decrease of the absorption features related to PCBM and an enhancement of those attributed to P3HT. Further, the region around the absorption peak of P3HT in the spectrum of the annealed film is slightly extended towards longer wavelengths while the shoulder present at around 600 nm, supposed to be resulting from interchain interactions,[17] becomes more pronounced. The presence of PCBM is known to quench the red band of the P3HT absorption while maintaining the absorption in the blue band. This is indicative for the disruption of the intermolecular packing structure of the P3HT chains and reduced density of aggregates that give rise to the red absorption.[18] The annealing process induces partial recovery of the ordered structure of the P3HT chains, which results in a red shift of the absorption features of P3HT. However, a slight blue-shift of the P3HT absorption features in the blend film also remains after annealing as compared to the pristine P3HT film. Similar behavior, but more pronounced, can be observed for the composite film prepared by successive spray deposition of the individual components. The strong blue-shift of the P3HT absorption features present in the spectrum of the as-prepared film indicates a disruption of the P3HT ordering by the PCBM. This means that the integrity of the initially sprayed P3HT film is not entirely preserved during the subsequent spraying cycle of PCBM. Quenching of the red band of the P3HT absorption in the successively sprayed film can therefore be seen as indicative for a penetration of PCBM into the P3HT layer and an intermixing of both materials. However, coarse intermixing of the materials within the photoactive layer due to interaction with residual solvent during deposition, described above to occur at a scale of a few tens of micrometers, cannot alone cause the quenching observed here. The intermixing has to occur at a nanometer scale, as to cause disruption of the P3HT chain ordering. It is therefore most likely that upon annealing, an additional fine intermixing takes place by interdiffusion of PCBM into P3HT, resulting in the formation of a morphology close to that of the conventional BHJ. It should be noted that the annealed film exhibits a significant red-shift of the P3HT peak wavelength upon partial recovery of the polymer chain ordering, bringing it very close to the position of its counterpart in the spectrum of the blend film.

In addition X-ray reflectivity measurements have been used to investigate the intermixing of the P3HT layer with the subsequently deposited PCBM molecules. In contrast to the optical absorption spectra, X-ray reflectivity measurements allow an accurate

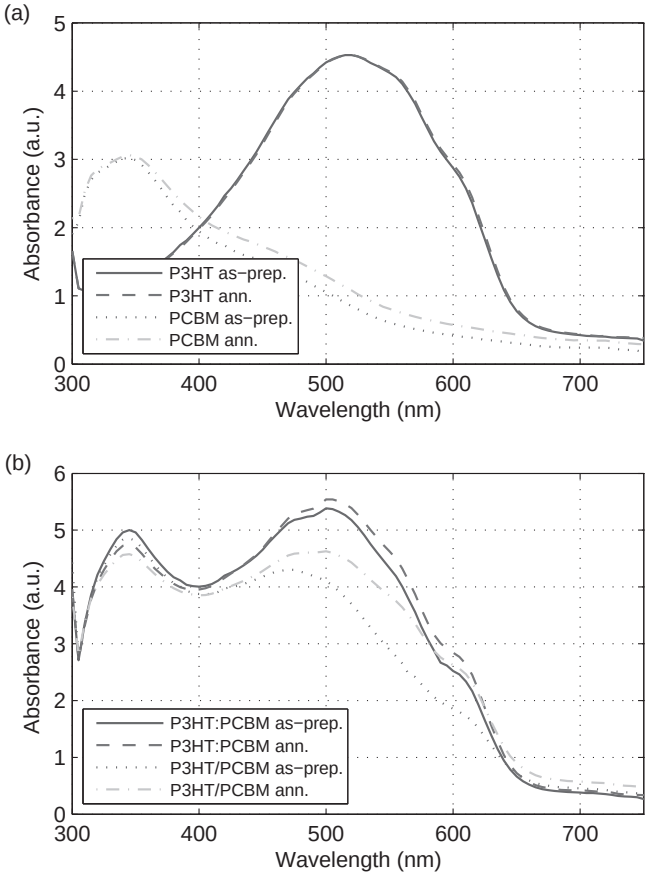

Figure 4. UV-vis absorption spectra of pristine P3HT (15 s) and PCBM (10 s) films (a) as well as composite P3HT:PCBM (20 s) blend and P3HT/PCBM (15/10 s) successively sprayed films (b) obtained before and after thermal post-deposition treatment of the samples. Quenching of the red band of the P3HT absorption in the successively sprayed film can be seen as indicative for a penetration of PCBM into the P3HT layer and an intermixing of both materials.

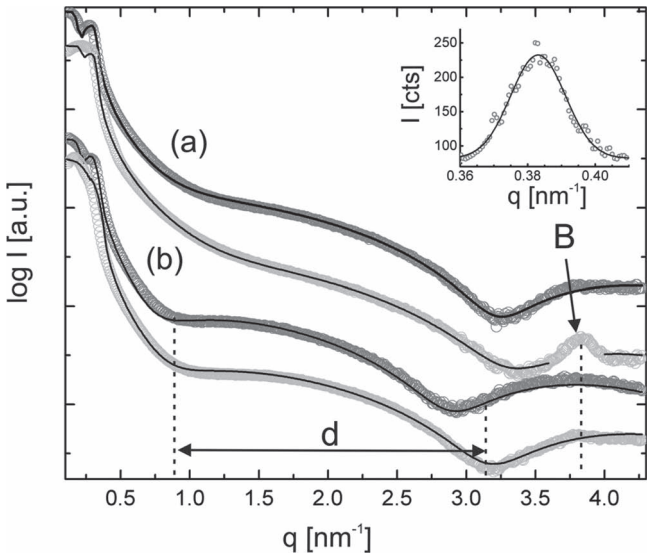

Figure 5. X-ray reflectivity curves of a) pure spray coated P3HT films and b) successive sprayed P3HT/PCBM layered films. Both the pristine (dark grey) and the annealed (bright grey) films are shown for the single and the multilayer films. The position of the Bragg peak from the crystalline structure of the P3HT is marked with "B". The thickness of a densely packed P3HT film at the substrate interface is seen in the intensity modulation marked with "d". The inset shows the exact position of the (100)-Bragg peak of the semicrystalline P3HT and the corresponding Gaussian fit.

determination of the film thickness of thin polymeric layers and reveal the inner film morphology of layered systems.[19,20] **Figure 5** shows the measured reflectivity curves together with the model fits for pristine and annealed P3HT films and for the layered P3HT/PCBM system. For angles larger than the critical angles of the materials used, which are in our case 0.159° and 0.146° for P3HT and PCBM, the incoming X-rays penetrate through the complete film. Therefore these measurements are not only sensitive to the bulk properties of the films but also reveal thin enrichment layers as they can be seen from the prominent long modulations in the reflectivity curves. Due to the high surface roughness of the films, the total film thickness is not seen by strong intensity modulations, which facilitates the detection of enrichment layers at the substrate. For the pristine P3HT films the corresponding Parrat simulations reveal an enrichment layer with a thickness of 2.3 nm, which increases to 2.6 nm after annealing. This enrichment layer is given by a layer of P3HT with a more dense packing, located at the substrate. Such a dense packing of P3HT polymer chains is not seen for spin-coated films and can hence be attributed to the spray coating technique, which leads to a physically accelerated deposition of the polymeric material on a hard substrate at elevated temperature. After annealing the enrichment layer gets less pronounced due to the rearrangement of the P3HT molecules. The resulting crystalline ordering of the P3HT molecules is seen from the well-defined Bragg reflection in the X-ray reflectivity curve of the annealed film (denoted with "B" in Figure 5). The inset in Figure 5 shows the corresponding Gaussian fit on a linear scale. The Bragg peak is centered at a position with a q_z-value of 3.83 nm^{-1}. This value corresponds to a structure size of 1.64 nm and is hence in very good agreement with the (100) Bragg peak of P3HT in an edge-on arrangement as reported by Kim et al.[21] The higher Bragg orders of this molecular arrangement appear at larger angles and cannot be resolved due to limitations in intensity. For the pure P3HT films the evolution of the Bragg peak clearly shows that the crystalline ordering can be introduced to the P3HT polymer matrix with an additional post-deposition annealing step. In contrast, for the P3HT/PCBM bilayer system an equivalent crystalline ordering as seen in the pure P3HT films was not achieved. No Bragg peak is found in the X-ray reflectivity data. Also the annealing has only a minor influence on the crystallinity of the firstly deposited P3HT and only a very weak indication of a Bragg peak is found in the X-ray reflectivity data. The absence of a well-defined (100) Bragg peak is a strong indication for a good penetration of the PCBM molecules into the P3HT matrix, which perturb the P3HT-lattice and hence prevent a crystalline ordering even after annealing. By using grazing incidence wide angle X-ray scattering (GIWAXS) a similar behavior was also found for spin-coated P3OT/CN-PPV bulk heterojunction films, which exhibited a less crystalline ordering as compared with the pristine films.[22] The already mentioned enrichment layer is seen in the successively sprayed P3HT/PCBM samples as well and shows a similar slight increase in thickness as it was found for the pure P3HT films. Combining the results of the optical absorption and the X-ray reflectivity measurements a significant penetration of the stepwise deposited P3HT and PCBM is found, which makes this fabrication routine very interesting for device applications, where a high interfacial area between the used materials is desired.

The morphology of the active layer was further studied by TEM investigations. The active layer can easily be identified as the region between the silicon substrate and the aluminum coating. In the active layer a percipient contrast was observed indicating the presence of two phases with an interface in the middle as shown in the TEM image **Figure 6**a. The same figure shows SAED patterns of two regions marked as "1" and "2". The first region 1, located in the domain adjacent to the aluminum´, showed a crystalline diffraction pattern with a d-spacing of 15.4 Å, which matches fairly well the d-value proposed by Li et al.[23] This indicates the domain adjacent to the aluminum to be highly crystalline PCBM. The other region labeled in Figure 6a as 2 turned out to be amorphous as is illustrated by the SAED pattern on bottom right. Subsequently, to identify the elemental composition of the active layer, EDX measurements were done in STEM mode. EDX spectra were acquired from four regions across the active layer labeled 1-4 in Figure 6b. The EDX spectra obtained, plotted in **Figure 7**, show the composition in the domain adjacent to aluminum (region 3 and 4) to be primarily of carbon and oxygen. This matches with the chemical formula of PCBM $C_{72}H_{14}O_2$. This domain is highly crystalline and together with the SAED experiments can be identified as PCBM. Region 1 and 2 located in the domain next to silicon show predominant signal of carbon and sulfur in accordance to the elements expected for P3HT, which has a chemical formula of $[C_{10}H_{14}S]_n$. A very weak oxygen signal is visible in the EDX data of the P3HT layer, which was also confirmed by EELS measurements. This very weak oxygen signal detected within the P3HT layer might be related to interdiffusion of PCBM

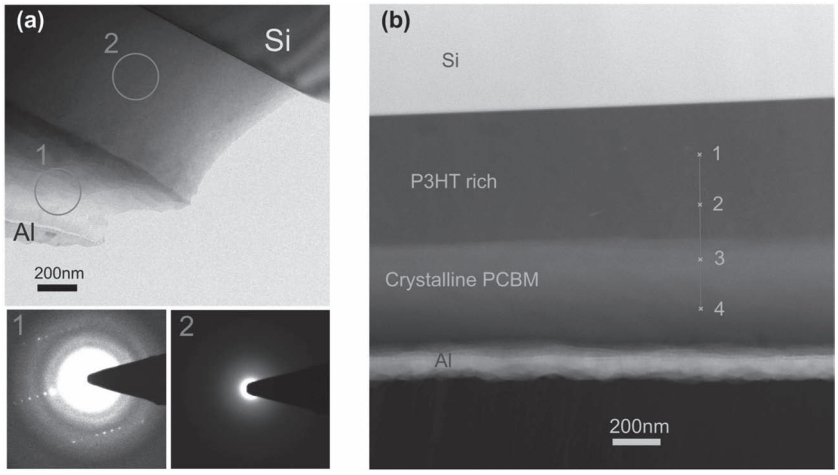

Figure 6. a) Above is a TEM image from a thin region in the active layer. Diffraction patterns were obtained from regions indicated 1 and 2 and are shown below on left for 1 and on right for 2. b) STEM image showing the active layer and the four spots 1, 2, 3, and 4 across the active layer from where point EDX spectra were acquired.

into this layer as suggested by,[11,12] or stem from oxidation of the sample surface prior to insertion into the microscope. To clarify that point, further investigations are required. Our TEM investigations further support the idea of PCBM diffusion into the P3HT layer. The absence of a clear diffraction pattern in the P3HT-rich region indicates the disruption of crystallinity, as proposed above by optical absorption and X-ray reflectivity analysis. We assume that the absence of any dominant oxygen signal, originating from the existence of PCBM, is due to the low concentration of PCBM throughout the entire region. DSIMS profiles of P3HT/dPCBM bilayers reported by Chen et al. showed only slight increase of PCBM concentration in the P3HT and no variation with depth upon annealing,[12] which is consistent with our assumption of low PCBM concentration in the P3HT-rich region.

2.3 Implementation in Organic Photodetectors

For a comprehensive evaluation of the deposition approach described here and its potential competitiveness with more conventional pre-deposition blending approaches, devices fabricated by both techniques must be directly compared in terms of common performance parameters. A set of OPDs was fabricated by successive multilayer spray deposition while varying deposition times of P3HT and PCBM for obtaining different compositions of the active layer. This was then compared to another set of OPDs fabricated by direct spray deposition of a P3HT:PCBM (1:1) blend while

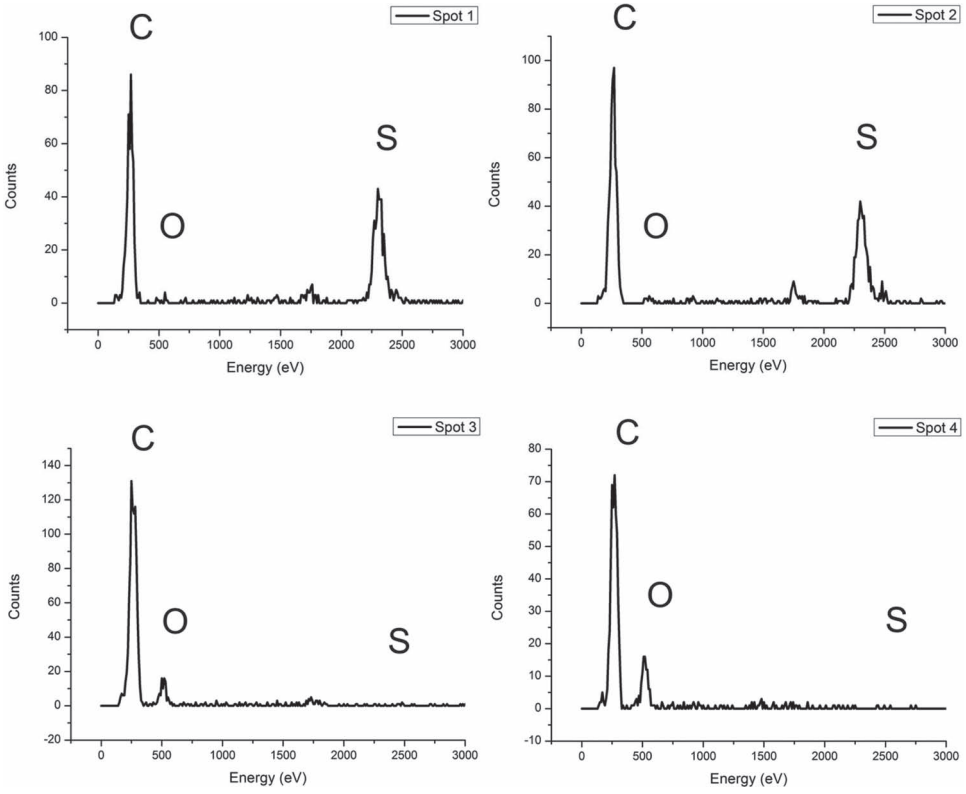

Figure 7. EDX spectra acquired from spots 1, 2, 3, and 4 labeled in Figure 6b.

varying deposition times to obtain different thicknesses of the active layer. Note that the performance of such spray-coated BHJ photodiodes matches the one of their spin-coated counterparts.[14,24] As the two device groups rely on an essentially different process of active layer formation, a direct comparison is rather difficult. For this reason and for the purpose of proving the competitiveness of our approach, we chose the parameter combination in each group leading to almost identical performance of the corresponding devices. This is fairly easy to accomplish due to the high flexibility in tuning layer composition and device performance by successive multilayer deposition (Supporting Information). Moreover, the two selected devices happened to be best out of their corresponding group. **Figure 8**a shows the IV-characteristics of device D6, fabricated by spraying a blend solution for 20 s, and device D7, fabricated by spraying a P3HT solution for 15 s followed by spraying a PCBM solution for 10 s. Note that the data points for each device type plotted in the figure correspond to averaged values from three individually sprayed diodes. The deviation within individual diodes of the same type is comparable for both deposition approaches. At –1 V reverse bias for example, the deviation for D6 is approx. 1.5% in the photocurrent and 24% in the dark current, whereas for D7 it is approx. 2.8% and 22% at the same conditions. This demonstrates the reproducibility and reliability of our deposition method. By looking at the IV-curves it becomes immediately obvious that both devices exhibit very similar behavior under dark as well as illuminated conditions. The conventional blend device D6 shows an on/off-ratio of around 6×10^4 and a dark current density of 4.3×10^{-5} mA cm^{-2} under –1 V reverse bias. For the successively sprayed device D7 one obtains an on/off-ratio of around 8.8×10^4 and a dark current density of 3×10^{-5} mA cm^{-2} under –1 V reverse bias, thereby slightly outperforming the blend device. However, both devices maintain a high on/off-ratio and relatively low dark current densities even at higher reverse bias, with on/off-ratios slightly below 10^4 and dark current densities below 4×10^{-4} mA cm^{-2} under –5 V reverse bias. In terms of external quantum efficiency, plotted in Figure 8b, both devices show almost identical behavior as expected. The spectral response is perfectly identical and the difference in the absolute values of up to 1% lies within the inaccuracy of the measurement setup.

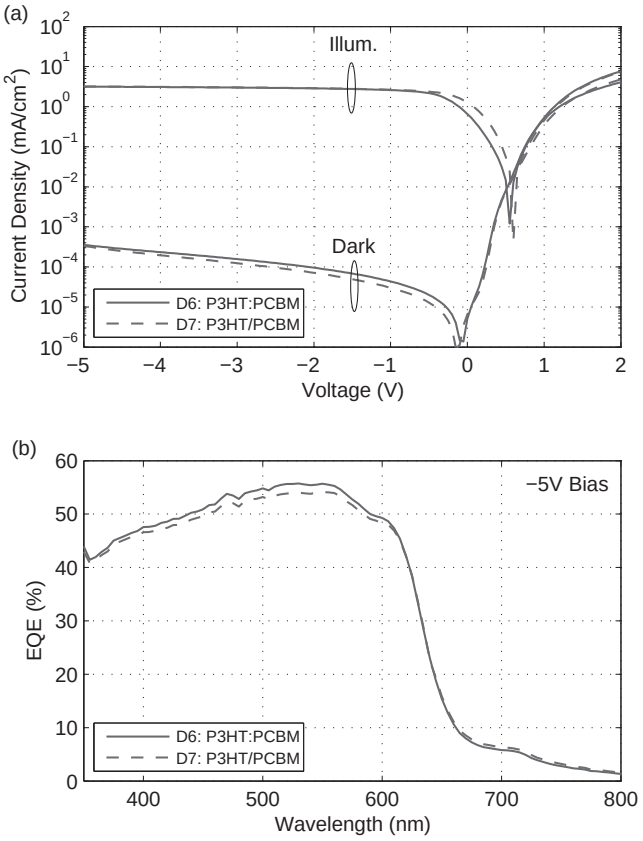

Figure 8. a) I–V characteristics of OPD D6, fabricated by spraying a blend solution for 20 s, and OPD D7, fabricated by spraying a P3HT solution for 15 s followed by spraying a PCBM solution for 10 s. The graph shows device behavior under dark as well as illuminated condition. b) Plot of the external quantum efficiency against wavelength for devices D6 and D7.

Based on these results, one can conclude that devices with active layers fabricated by successive spray deposition of the individual components exhibit a performance comparable to conventional BHJ devices in which the active layer is rigorously blended in advance. At first glance, this may not seem very intuitive. Considering an average droplet size of a few tens of micrometers in this kind of spray technology, one would expect the intermixing to occur on a scale several orders of magnitude larger than in a BHJ architecture which would lead to a decreased donor/acceptor interface area and hence lower exciton dissociation efficiency. Based on the analysis carried out so far, we attribute the good device performance to two main factors. The existance of a P3HT-rich layer at the hole-extraction interface and a PCBM-rich layer at the electron extraction interface leads to an increased charge carrier selectivity at the respective electrodes. Primarily however, although the spray process itself is expected to generate a coarse intermixing of the two materials on the scale of the droplet size, a further intermixing occurs at the nanometer scale due to diffusion of PCBM into the underlying P3HT layer. Note that in addition to the thermal post-deposition treatment of our devices, there is a short annealing cycle during the deposition phase itself, since deposition is performed at elevated substrate temperature (ca. 150 °C) for accelerated drying of droplets. Similar findings were previously reported as solid-solid intermixing in bilayer devices prepared by stamping transfer,[25] or as thermally induced interdiffusion demonstrated in devices prepared by consecutively spin-cast layers of P3OT and PCBM from different solvents.[26] Spontaneous formation of a BHJ-like nanomorphology upon annealing of model bilayer systems was recently shown to result from PCBM diffusion into disordered P3HT domains without disruption of the crystalline P3HT domains.[10,12] In contrast to this, our findings suggest that diffusion of PCBM into the P3HT layer disrupts chain ordering. We believe that this discrepancy arises from our significantly different fabrication approach. The interaction with the residual solvent during deposition of PCBM leads to partial dissolving and swelling of the P3HT layer, which together with the elevated temperature enables PCBM diffusion not only into disordered P3HT domains but also into previously crystalline domains. While all results presented here are specific to the common P3HT/PCBM material

system, the generality of the proposed fabrication approach for different material systems still has to be investigated.

3. Conclusion

We have introduced an alternative deposition approach for the preparation of organic heterojunction photoactive layers by successive spray deposition of the donor and acceptor materials from pristine solutions. The partial dissolving of previously deposited underlying layers was carefully examined using optical and atomic force microscopy. It was shown that P3HT-rich and PCBM-rich layers are expected to form at the vicinity of the hole-extraction and electron-extraction layers, respectively. Optical absorption spectra as well as X-ray reflectivity measurements were utilized to indicate the disruption of P3HT ordering by the subsequently deposited PCBM. Further, cross-sectional TEM investigations, including material analysis with SEAD and EDX, were performed to further support the idea of PCBM penetration into the P3HT layer and the intermixing of both materials within the active layer. Based on performance characteristics of the fabricated organic photodetectors, we can conclude that devices with active layers prepared by successive spray deposition of the individual components exhibit a performance comparable to and can potentially outperform conventional BHJ devices in which the active layer is rigorously blended in advance. Moreover, separate handling of the individual components and their deposition from distinct solutions enables an enhanced control of the active layer composition and hence increases the ability of tuning device characteristics. Although we focused here on the fabrication of organic photodiodes, the proposed fabrication routine is very interesting for different device applications, which require an intermixed layer of different materials while allowing for convenient control over its composition. Our results illustrate the significance of altered fabrication routines on processes predominantly taking place at the nanometer scale. Such processes, like exciton dissociation and charge transport in domains of an interpenetrating network of donor and acceptor molecules, are critical for device performance. From a practical perspective, devices with excellent performance could be fabricated in simple and controllable ways using an industrial relevant high-throughput process.

4. Experimental Section

Experimental Setup: The experimental setup used to fabricate all samples was composed of an air atomizing spray gun in a vertical static arrangement with respect to a heatable substrate. The main spray parameters to be adjusted for obtaining desired spray characteristics were material flow rate, atomizing gas (N_2) pressure, nozzle-to-sample distance and substrate temperature. A commercially available spray gun (Krautzberger GmbH, Germany) with 0.5 mm orifice diameter was utilized for the atomization of the coating solution. The atomizing gas (N_2) pressure was kept below 1 bar throughout all experiments in order to obtain the desired spray characteristics and a uniform spray pattern across the area of interest. More details regarding spray setup and parameters were discussed previously.[15]

Solution Preparation: Solutions of the pristine acceptor and donor materials were prepared in o-dichlorobenzene (o-DCB) with 1 wt% concentration using regioregular poly(3-hexylthiophene-2,5-diyl) (P3HT) (Rieke Metals Inc.) and [6,6]-phenyl C61 butyric acid methyl ester (PCBM) (Solenne B.V.), respectively. The blend solution consisting of a P3HT:PCBM (1:1) mixture, used for the fabrication of reference devices, was similarly prepared in o-DCB with 1 wt% concentration.

Device Fabrication: For the fabrication of our organic photodiodes, pre-patterned ITO-glass substrates were cleaned by sonication in acetone followed by isopropanol. A PEDOT:PSS aqueous dispersion (CLEVIOS P VP CH 8000) was deposited by spin coating at 2000 rpm for 20 s and then dried on a hot plate at 150 °C for 15 min. The active layers were then deposited from the desired solutions using our above described spray setup. Finally, the cathode consisting of 1 nm LiF and 100 nm Al was thermally evaporated on top. Samples were placed on a hot plate for annealing at 150 °C for 15 min. either before or after deposition of the metal top electrode. The active area of each diode was defined by bottom and top electrode geometry to be either 25 mm^2 or 9 mm^2. Note that the organic active layers were deposited in ambient conditions, while only annealing steps and device encapsulation were performed under controlled nitrogen atmosphere inside a glove box.

Active Layer Characterization: Depending on the refractive index of the materials used X-ray reflectivity measurements allow a film composition analysis parallel to the sample normal and can be used to investigate the crystallinity of the semi-crystalline P3HT. The X-ray reflectivity data were taken at a Siemens D5000 diffractometer at a wavelength of 0.154 nm (Cu-Kα radiation) in an angular range from 0° to 6° using a θ–2θ geometry. Silicon substrates were used in order to minimize the substrate influence on the recorded reflectivity curve. Since the sample preparation was identical to that of the final device prepared on ITO substrates, same film morphologies can be expected. In addition a knife edge was used to limit the beam size and to reduce the background. The reflected intensity was recorded via a point detector, which was protected by an automatic beam absorber. For analysis the reflectivity data were fitted with the Parrat32 reflectivity simulation software.[27]

For TEM investigations samples were spray coated as described above on a silicon substrate because of the relative ease of cross sectional sample preparation for a silicon substrate. In addition, for protecting the active layer from the rigors of TEM sample preparation a thin aluminum layer (~100 nm) was deposited on top of the active layer. The material was cut into slices, inserted in a brass tube, and thinned by mechanical grinding and dimpling. Subsequently precision ion polishing was employed for the final thinning process using a Gatan Precision Ion Polishing System operated with argon ions at 3keV and liquid nitrogen cooling. The TEM measurements were performed on a FEI TITAN 80–300 operated at 80 and 300 keV. Since the specimen were surprisingly stable upon irradiation with the electron beam, images shown in this work were acquired while operating the TEM at 300 keV as it allowed investigation of thicker specimen regions. Scanning transmission electron microscopy (STEM) in high angular annular dark field (HAADF) mode was employed with a convergence semi-angle of 9.5 mrad to acquire images with z-contrast dependency. In conjunction, selected area electron diffraction (SAED), energy dispersive X-ray spectroscopy (EDX) and electron energy loss spectroscopy (EELS) were employed for analytical measurements.

Device Characterization: Optical absorption spectra as well as external quantum efficiency (EQE) were measured using a chopped 300 W xenon arc research source passing through an Oriel Cornerstone 260 1/4 m monochromator and a calibrated silicon photodiode with pre-amplifier connected to an Oriel Merlin digital lock-in radiometry system. For the IV-characterization of the OPDs, dark current measurements were performed inside a dark box while photocurrent measurements were performed under illumination with a tungsten halogen source at 100 mW cm^{-2}.

Supporting Information

Supporting Information is available from the Wiley Online Library or from the author.

Acknowledgements

This work was partially supported by the DFG within the German Excellence Initiative via the cluster of Excellence Nanosystems Initiative Munich (NIM).

Received: February 24, 2012
Published online: June 5, 2012

[1] G. Li, V. Shrotriya, J. Huang, Y. Yao, T. Moriarty, K. Emery, Y. Yang, *Nat. Mater.* **2005**, *4*, 864.
[2] T. Erb, U. Zhokhavets, G. Gobsch, S. Raleva, B. Stühn, P. Schilinsky, C. Waldauf, C. J. Brabec, *Adv. Funct. Mater.* **2005**, *15*, 1193.
[3] W. Ma, C. Yang, X. Gong, K. Lee, A. J. Heeger, *Adv. Funct. Mater.* **2005**, *15*, 1617.
[4] M. Campoy-Quiles, T. Ferenczi, T. Agostinelli, P. G. Etchegoin, Y. Kim, T. D. Anthopoulos, P. N. Stavrinou, D. D. C. Bradley, J. Nelson, *Nat. Mater.* **2008**, *7*, 158.
[5] C.-W. Liang, W.-F. Su, L. Wang, *Appl. Phys. Lett.* **2009**, *95*, 133303.
[6] A. Kumar, G. Li, Z. Hong, Y. Yang, *Nanotechnology* **2009**, *20*, 165202.
[7] D. H. Wang, H. K. Lee, D.-G. Choi, J. H. Park, O. O. Park, *Appl. Phys. Lett.* **2009**, *95*, 043505.
[8] A. L. Ayzner, C. J. Tassone, S. H. Tolbert, B. J. Schwartz, *J. Phys. Chem. C* **2009**, *113*, 20050.
[9] L. M. Chen, Z. Hong, W. L. Kwan, C.-H. Lu, Y. F. Lai, B. Lei, C. P. Liu, Y. Yang, *ACS Nano* **2010**, *4*, 4744.
[10] N. D. Treat, M. A. Brady, G. Smith, M. F. Toney, E. J. Kramer, C. J. Hawker, M. L. Chabinyc, *Adv. Energy Mater.* **2011**, *1*, 82.
[11] J. S. Moon, C. J. Takacs, Y. Sun, A. J. Heeger, *Nano Lett.* **2011**, *11*, 1036.
[12] D. Chen, F. Liu, C. Wang, A. Nakahara, T. P. Russell, *Nano Lett.* **2011**, *11*, 2071.
[13] C. Girotto, B. P. Rand, J. Genoe, P. Heremans, *Sol. Energy Mater. Sol. Cells* **2009**, *93*, 454.
[14] A. Abdellah, D. Baierl, B. Fabel, P. Lugli, G. Scarpa, *Nanotechnology, 2009. IEEE-NANO 2009. 9th IEEE Conf.* **2009**, *978-981-08-3694-8*, 831.
[15] A. Abdellah, B. Fabel, P. Lugli, G. Scarpa, *Org. Electron.* **2010**, *11*, 1031.
[16] D. Chirvase, J. Parisi, J. Hummelen, V. Dyakonov, *Nanotechnology* **2004**, *15*, 1317.
[17] P. J. Brown, D. S. Thomas, A. Köhler, J. S. Wilson, J.-S. Kim, C. M. Ramsdale, H. Sirringhaus, R. H. Friend, *Phys. Rev. B* **2003**, *67*, 064203.
[18] Y. Kim, S. A. Choulis, J. Nelson, D. D. C. Bradley, S. Cook, J. R. Durrant, *J. Mater. Sci.* **2005**, *40*, 1371.
[19] M. A. Ruderer, E. Metwalli, W. Wang, G. Kaune, S. V. Roth, P. Müller-Buschbaum, *ChemPhysChem* **2009**, *10*, 664.
[20] G. Kaune, P. Müller-Buschbaum, *Phys. Status Solidi (RRL) - Rapid Research Lett.* **2010**, *4*, 52.
[21] H. J. Kim, J. H. Park, H. H. Lee, D. R. Lee, J.-J. Kim, *Org. Electron.* **2009**, *10*, 1505.
[22] M. A. Ruderer, S. M. Prams, M. Rawolle, Q. Zhong, J. Perlich, S. V. Roth, P. Müller-Buschbaum, *J. Phys. Chem. B* **2010**, *114*, 15451.
[23] L. Li, G. Lu, S. Li, H. Tang, X. Yang, *J. Phys. Chem. B* **2008**, *112*, 15651.
[24] S. F. Tedde, J. Kern, T. Sterzl, J. Furst, P. Lugli, O. Hayden, *Nano Lett.* **2009**, *9*, 980.
[25] D. H. Wang, D. G. Choi, K. J. Lee, S. H. Im, O. Ok Park, J. H. Park, *Org. Electron.* **2010**, *11*, 1376.
[26] M. Kaur, A. Gopal, R. M. Davis, J. R. Heflin, *Sol. Energy Mater. Sol. Cells* **2009**, *93*, 1779.
[27] L. G. Parratt, *Phys. Rev.* **1954**, *95*, 359.